Parametric spin pumping into an antiferromagnetic insulator

Taiki Numata,[1] Hiroki Hayashi,[1] Hiroto Sakimura,[1,2] and Kazuya Ando[1,3,*]

[1]*Department of Applied Physics and Physico-Informatics, Keio University, Yokohama 223-8522, Japan*
[2]*School of Materials and Chemical Technology, Tokyo Institute of Technology, Tokyo 152-8552, Japan*
[3]*Center for Spintronics Research Network (CSRN), Keio University, Yokohama 223-8522, Japan*

(Received 2 June 2019; revised manuscript received 12 July 2019; published 21 October 2019)

We report the observation of spin transport through antiferromagnetic insulators using spin pumping driven by short-wavelength magnons. The short-wavelength magnons are excited by parametric pumping in a $Pt/NiO/Y_3Fe_5O_{12}$ trilayer. The parametrically excited magnons in the $Y_3Fe_5O_{12}$ layer inject a spin current into the NiO layer, which is detected electrically using the inverse spin Hall effect in the Pt layer. We found that the spin-pumping efficiency of the parametrically excited magnons in the $Pt/NiO/Y_3Fe_5O_{12}$ film is nearly an order of magnitude smaller than that in the $Pt/Y_3Fe_5O_{12}$ film. The suppression of the parametric spin-pumping efficiency induced by inserting the NiO layer is comparable to that of the FMR spin-pumping efficiency. We further found that the suppression of the spin-pumping efficiency due to the NiO insertion for the dipole-exchange magnons with the wave number of $k \sim 10^3 - 10^4$ cm^{-1} is more significant than that for the exchange magnons with $k \sim 10^5$ cm^{-1}. This difference is attributed to two-magnon scattering and spin pinning due to antiferromagnetic grains in the NiO layer. These results provide insight into the understanding of the spin pumping into antiferromagnetic insulators.

DOI: 10.1103/PhysRevB.100.144430

I. INTRODUCTION

The physics of spin currents has been the fundamental building block of spintronics for the past two decades [1]. Spin currents can be carried by electrons and magnons in metals, semiconductors, and insulators. The interconversion between electron and magnon spin currents induces a variety of phenomena in metal/insulator heterostructures, opening the field of insulator spintronics [2,3]. Recently, a number of surprising effects have been found in studies covering spin transport in antiferromagnetic insulators, such as an enhancement of a spin current upon the introduction of a thin antiferromagnetic layer [4,5]. The exploration of spin currents involving antiferromagnetic insulators has set a new direction in spintronics [4–17].

Spin transport in antiferromagnetic insulators has been mainly studied by spin Seebeck effect [4,9] and microwave spin pumping [5–8]. The spin Seebeck effect in a heavy-metal/antiferromagnet/ferromagnet structure injects a spin current into the antiferromagnetic layer, and the spin current is detected through the inverse spin Hall effect (ISHE) in the heavy metal layer [19–21]. In the spin Seebeck effect, the spin current is injected by thermally generated magnons with a wide range of frequencies and wave numbers in the ferromagnetic layer [3,22]. In contrast to the spin Seebeck effect, the frequency and wave number of the magnons responsible for the spin current can be controlled in the spin pumping, where a spin current is generated by magnons excited by a microwave [23,24]. Previous studies on the spin pumping in heavy-metal/ferromagnet structures have demonstrated wave-number-dependent conversion efficiency from the microwave absorbed by the ferromagnet into the generated spin current, such as efficient spin pumping driven by magnetostatic surface modes [25] and systematic variation of the conversion efficiency of short-wavelength magnons [26]. However, the spin pumping into the antiferromagnetic insulators has been limited to the spin pumping driven by the ferromagnetic resonance (FMR), or the uniform magnetization precession. The magnon wave number dependence of the spin-pumping efficiency into antiferromagnetic insulators has not been clarified.

In this paper, we investigate the spin pumping in a $Pt/NiO/Y_3Fe_5O_{12}$ (Pt/NiO/YIG) trilayer under parametric excitation. The parametric excitation allows us to excite magnons with nonzero wave numbers, enabling us to study the transport of spins pumped by short-wavelength magnons. The parametric excitation process involves the splitting of a microwave photon with pumping frequency f_0 into a pair of magnons with one-half of the pumping frequency $f_0/2$ and oppositely oriented wave vectors $\mathbf{k} \neq \mathbf{0}$ through a virtual excitation of a uniform magnon, as shown in Fig. 1(a). The wave vector of the parametric magnons can be tuned by shifting the magnon dispersion in the momentum-frequency space by changing an external magnetic field. By measuring the spin pumping driven by the parametrically excited magnons [26,28–30], we found that the spin-pumping efficiency of the parametrically excited magnons in the $Pt/NiO/Y_3Fe_5O_{12}$ film is nearly an order of magnitude smaller than that in the $Pt/Y_3Fe_5O_{12}$ film. We further found that the suppression of the spin-pumping efficiency due to the NiO insertion for the dipole-exchange magnons with the wave number of $k \sim 10^3 - 10^4$ cm^{-1} is more significant than that for the exchange magnons with $k \sim 10^5$ cm^{-1}. This difference is attributed to

*Corresponding author: ando@appi.keio.ac.jp

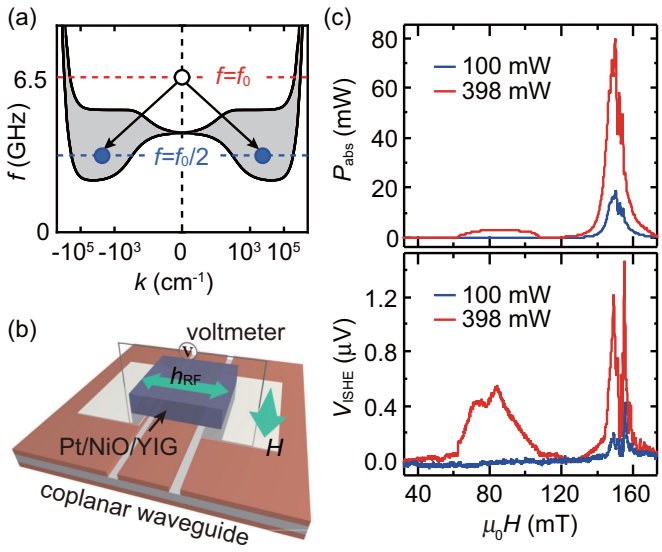

FIG. 1. (a) The magnon dispersion for a YIG film with a schematic of parametric excitation. f_0 is the applied microwave frequency. (b) A schematic illustration of the experimental setup, where H is the external magnetic field and h_{RF} is the microwave magnetic field. The microwave absorption intensity P_{abs} in the sample was determined by measuring S_{21} using a vector network analyzer, $P_{abs} = (\Delta|S_{21}|^2/|S_{21}^0|)P_{in}$, where $|S_{21}^0|$ represents the ratio between the incident and transmitted microwave power without magnetic resonance. $\Delta|S_{21}|^2$ is the change ratio of the transmitted microwave power [18]. (c) Magnetic field H dependence of the microwave absorption intensity P_{abs} and ISHE voltage V_{ISHE} measured for the Pt/NiO/YIG trilayer at the microwave frequency of $f_0 = 6.5$ GHz with the power of $P_{in} = 100$ mW (the solid curve in blue) and 398 mW (the solid curve in red).

two-magnon scattering and spin pinning due to antiferromagnetic grains in the NiO layer.

II. EXPERIMENTAL METHODS

The standard system to study the spin pumping induced by the parametric excitation is a $Pt/Y_3Fe_5O_{12}$ (Pt/YIG) bilayer, where the exceptionally low magnetic damping of the YIG layer allows us to induce nonlinear spin dynamics [31]. To study the spin transport in antiferromagnetic NiO induced by the parametric excitation, we fabricated a trilayer film, where a thin NiO layer is inserted between the Pt and YIG layers. The single-crystalline YIG (111) film with a thickness of 28 μm was grown by a liquid phase epitaxy on a $Gd_3Ga_5O_{12}$ (111) substrate (a 2×2 mm square shape). Then, the NiO layer was deposited on the YIG layer by sputtering in an Ar atmosphere. In the film, the thickness of the NiO layer is 4 nm, which allows us to measure the spin transport across antiferromagnetic NiO at room temperature. In the Pt/NiO/YIG trilayer, a spin current injected into the Pt layer decreases with increasing the NiO thickness because of the spin decay in the NiO layer, while, by decreasing the NiO thickness, the blocking temperature and Néel temperature of the NiO layer decreases. In the NiO film with the thickness of 4 nm, the blocking temperature and Néel temperature are above room temperature [32]. On top of the NiO layer, the Pt layer with a thickness of 7.5 nm was sputtered in an Ar atmosphere.

For the spin-pumping measurement, the sample was placed at the center of a coplanar waveguide, where a microwave signal was applied to the input signal line as shown in Fig. 1(b). The signal line is 200-μm wide and the gaps between the signal line and the ground lines were designed to match the characteristic impedance of 50 Ω. Two electrodes were attached to the Pt layer, and an in-plane external magnetic field H was applied parallel to the signal line. In the Pt/NiO/YIG trilayer film, under magnetic resonance conditions, magnons excited by the microwave drive the spin pumping, which emits a spin current into the NiO layer. When the spin current carried by magnons in the NiO layer reaches the Pt layer, the spin current is converted into an electric voltage via the ISHE. We measured the ISHE voltage V_{ISHE} and microwave absorption intensity P_{abs}, induced by the magnetic resonance, using a nanovoltmeter and a vector network analyzer, respectively. For comparison, we also measured V_{ISHE} and P_{abs} for a Pt(7.5)/YIG(28 μm) bilayer. The magnetic properties of the YIG layer are the same for the Pt/NiO/YIG and Pt/YIG films because these films were cut from the same YIG film. All the experiments were performed at room temperature.

III. RESULTS AND DISCUSSION

Figure 1(c) shows $\mu_0 H$ dependence of the P_{abs} and V_{ISHE} signals measured for the Pt/NiO/YIG trilayer at a microwave frequency $f_0 = 6.5$ GHz. The P_{abs} and V_{ISHE} signals observed around $\mu_0 H = 150$ mT are induced by the microwave absorption and ISHE voltage due to the FMR and long-wavelength spin-wave resonance in the YIG layer. By increasing the microwave excitation power from 100 mW to 398 mW, additional signals appear in the P_{abs} and V_{ISHE} spectra in the magnetic field range of 50 mT $< \mu_0 H <$ 110 mT, as shown in Fig, 1(c). These signals in P_{abs} and V_{ISHE} are induced by the parametric excitation, where the microwave creates pairs of magnons with the frequency of $f_0/2$ and opposite wave vectors $\mathbf{k} \neq \mathbf{0}$ [see Fig. 1(a)]. Since V_{ISHE} is generated by the spin current injected into the Pt layer, the clear signal in the V_{ISHE} spectrum shows that the spin current pumped by the $\mathbf{k}\neq\mathbf{0}$ magnons travels across the antiferromagnetic NiO layer.

In Fig. 2, we show the $\mu_0 H$ dependence of P_{abs} and V_{ISHE} induced by the parametrically excited magnons for the Pt/YIG and Pt/NiO/YIG films at various excitation powers P_{in}. Figure 2 shows that the P_{abs} and V_{ISHE} signals jump around $\mu_0 H = 50$ mT. Figure 2 also shows that the field $H_{jump}(P_{in})$ where P_{abs} and V_{ISHE} change abruptly depends on the microwave excitation power P_{in}. The drastic change in P_{abs} and V_{ISHE} at $H = H_{jump}(P_{in})$ is caused by a drastic change of the wave number of the primary magnons excited by the parametric excitation [26]. Under the parametric pumping, the wave number k of the primary magnons depends on the magnetic field H. At $H < H_{jump}$, only exchange magnons with $k \sim 10^5$ cm^{-1} can be excited, since no state of dipole-exchange magnons is available at $f_0/2$. By increasing H, the magnon dispersion shifts in momentum-frequency space, and at $H > H_{jump}$, dipole-exchange magnons with $k \sim 10^3 - 10^4$ cm^{-1} are excited by the microwave. In Fig. 3(a), we show the H dependence of the wave vector $\mathbf{k}$ of the primary excited

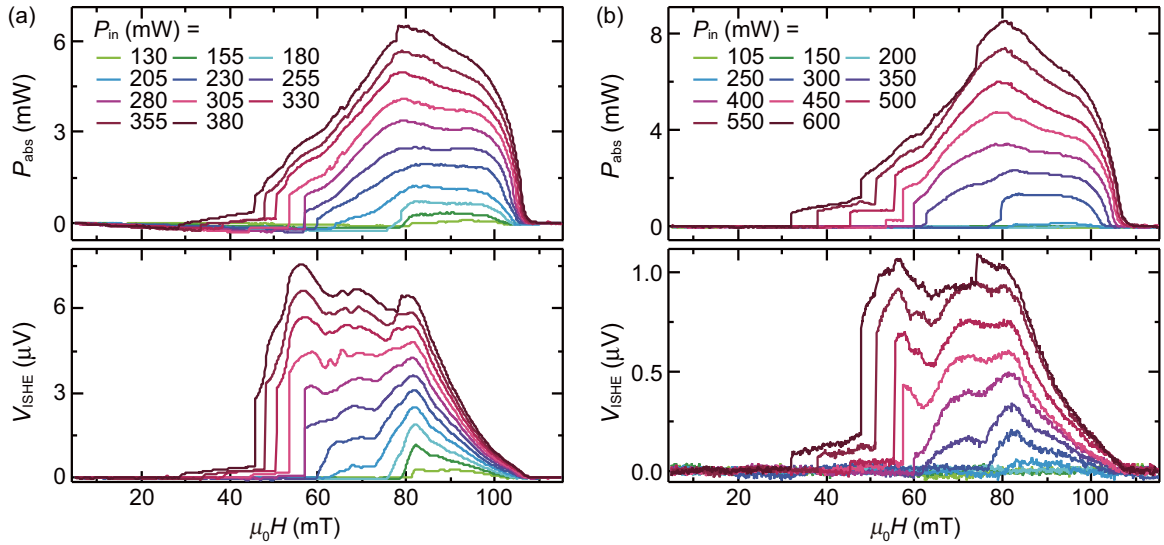

FIG. 2. Magnetic field H dependence of the microwave absorption intensity P_{abs} and ISHE voltage V_{ISHE} for the (a) Pt/YIG bilayer and (b) Pt/NiO/YIG trilayer measured at $f_0 = 6.5$ GHz with various excitation powers P_{in}. In the present study, the microwave excitation power P_{in} is defined as the power provided by the network analyzer. The microwave power applied to the sample, P_{app}, is suppressed from P_{in}: $P_{app} = \beta P_{in}$. Since the suppression factor β is hard to control in our experimental setup, β is different in different experiments, and therefore it is difficult to compare the data measured at the same P_{in} for different samples. This is the reason why the P_{abs} and V_{ISHE} signals measured at different P_{in} for the Pt/YIG bilayer and Pt/NiO/YIG trilayer are shown.

magnons at the threshold power, $P_{in} = P_{th}$. This result was obtained by finding k and θ_k that minimize the parametric pumping threshold $h_{th}(\mathbf{k}) = \eta_{\mathbf{k}}/V_{\mathbf{k}}$ using the coupled lateral mode theory [27]. Here, θ_k is the angle between $\mathbf{k}$ and $\mathbf{H}$, $\eta_{\mathbf{k}}$ is the damping of the magnon with the momentum $\hbar\mathbf{k}$, and $V_{\mathbf{k}}$ is the coupling strength between the uniform mode and a pair of $\pm\mathbf{k}$ magnons. The H dependence of the magnon damping $\eta_{\mathbf{k}}$ at 6.5 GHz was determined to reproduce the H dependence of the threshold power [see Fig. 3(b)] [27]. Figure 3(a) shows that dipole-exchange magnons are primary excited when $\mu_0 H > 57$ mT and exchange magnons are primary excited when $\mu_0 H < 57$ mT at $P_{in} = P_{th}$. The magnetic field where the primary magnon mode is changed corresponds to $H_{jump}(P_{in})$, where P_{abs} and V_{ISHE} change abruptly [26]. At low P_{in}, the P_{abs} and V_{ISHE} signals were observed only at $H > H_{jump}$ as shown in Fig. 2. The reason for this is that the threshold power of the parametric excitation increases with the wave number of the primary magnon mode [27], and thus only dipole-exchange magnons can be excited at low excitation powers. At high P_{in}, as shown in Fig. 2, $H_{jump}(P_{in})$ decreases with increasing P_{in}, which is caused by nonlinear effects [26]. Figure 2 also shows that P_{abs} and V_{ISHE} signals disappear at $\mu_0 H > 110$ mT. At this field, the parametric pumping excites magnons at the bottom of the dispersion, and therefore there is no state at $f_0/2$ when $\mu_0 H > 110$ mT.

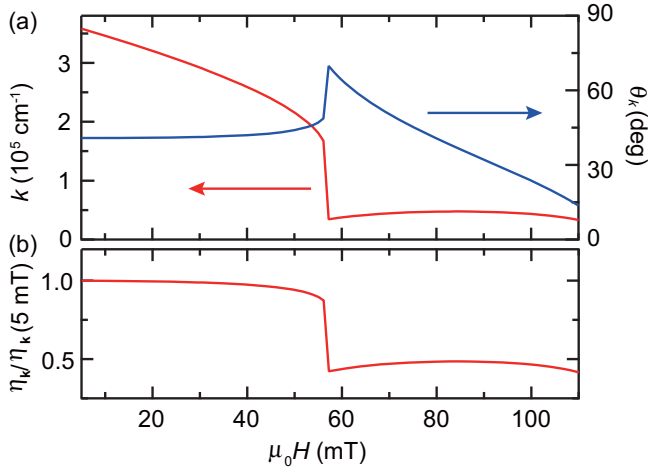

FIG. 3. (a) The calculated $\mu_0 H$ dependence of the wave number k, and the angle θ_k between $\mathbf{k}$ and $\mathbf{H}$ of the parametrically excited magnons at the threshold power under the 6.5 GHz microwave application. The calculated curves were obtained using the saturation magnetization $\mu_0 M_s = 198$ mT, $B/A = 3$, $k_c = 8.5 \times 10^7$ m^{-1}, and the exchange stiffness constant $D = 1.05 \times 10^{-5}$ m^2/s [26] (for details, see Ref. [27]). (b) $\mu_0 H$ dependence of the magnon damping $\eta_{\mathbf{k}}$ at 6.5 GHz. $\eta_{\mathbf{k}}$(5 mT) is the damping at $\mu_0 H = 5$ mT.

Figure 2 also shows that the spectral shape of V_{ISHE} is clearly different from that of P_{abs} for both samples. This indicates that the spin-pumping efficiency of the parametric magnon depends on the magnon wave number, which is consistent with previous reports [26,28]. To characterize the spin-pumping efficiency, we calculated $\kappa(H) \equiv V_{ISHE}(H)/P_{abs}(H)$ [26,28]. The highest value of the spin-pumping efficiency is $\kappa(\mu_0 H = 55\ \text{mT}) = 2.0\ \mu\text{V/mW}$ for the Py/YIG and $\kappa(\mu_0 H = 55\ \text{mT}) = 0.25\ \mu\text{V/mW}$ for the Py/NiO/YIG. The spin-pumping efficiency of the Pt/NiO/YIG is nearly an order of magnitude smaller than that of the Pt/YIG, as expected for the spin-current decay in the NiO layer. The suppression of the parametric spin-pumping efficiency due to the insertion of

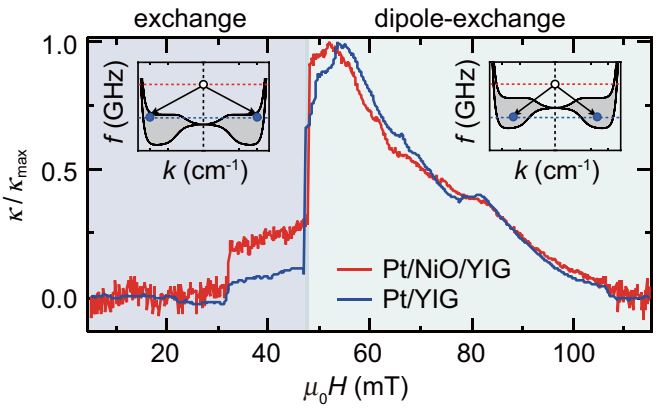

FIG. 4. Magnetic field H dependence of the spin-pumping efficiency κ/κ_{max} for the Pt/YIG bilayer at $P_{in} = 365$ mW (the solid curve in blue) and the Pt/NiO/YIG trilayer at $P_{in} = 600$ mW (the solid curve in red) measured at $f_0 = 6.5$ GHz. Here, $\kappa = V_{ISHE}/P_{abs}$, and κ_{max} is the maximum value of κ. To directly compare κ, we plot κ measured at the microwave powers at which the P_{abs} and V_{ISHE} signals are observed in the field range of 30 mT $< \mu_0 H <$ 110 mT in the Pt/NiO/YIG and Pt/YIG films. At $P_{in} = 365$ mW for the Pt/YIG and 600 mW for the Pt/NiO/YIG, $H_{jump}(P_{in})$, as well as the field range where the spin-pumping signal is observed, is the same between the Pt/NiO/YIG and Pt/YIG films. This allows us to directly compare the spin-pumping efficiency of exchange and dipole-exchange magnons in the two films. Although the frequency of the magnons excited in the present experiment is within the frequency range of the surface mode (see the inset), the transverse parametric pumping excites exchange magnons with large wave numbers, rather than the surface mode with relatively small wave numbers [27,33].

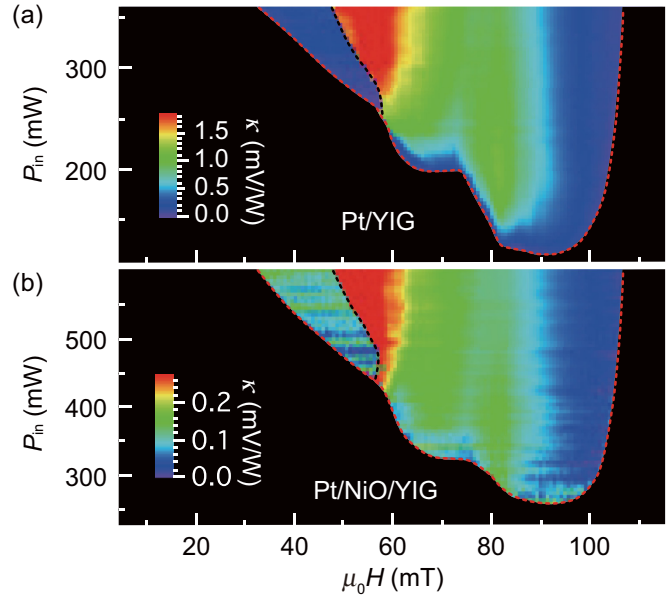

FIG. 5. A two-dimensional plot of the spin-pumping efficiency κ as a function of $\mu_0 H$ and P_{in} for the (a) Pt/YIG bilayer and (b) Pt/NiO/YIG trilayer. The dashed curve in red denotes the threshold power of the parametric excitation. The dashed curve in black is $H_{jump}(P_{in})$, the field where the primary excited magnons switch between dipole-exchange and exchange magnons.

the 4-nm-thick NiO layer is comparable to that of the FMR spin-pumping efficiency [5–7].

We found that the change of the spin-pumping efficiency due to the NiO insertion depends on the wave number of the parametrically excited magnons. In Fig. 4, we show the $\mu_0 H$ dependence of the spin-pumping efficiency $\kappa(H)/\kappa_{max}$ for the Pt/YIG bilayer and Pt/NiO/YIG trilayer, where κ_{max} is the maximum value of $\kappa(H)$. In Fig. 4, exchange magnons with $k \sim 10^5$ cm^{-1} and dipole-exchange magnons with $k \sim 10^3 - 10^4$ cm^{-1} are excited at $\mu_0 H < 48$ mT and $\mu_0 H > 48$ mT, respectively. The magnetic field where the primary mode switches is smaller than that shown in Fig. 3, which is due to the P_{in} dependence of $H_{jump}(P_{in})$ (see Fig. 2). Here, the spin-pumping efficiency, κ, jumps at $H_{jump}(P_{in})$ because of the wave-vector-dependent spin-pumping efficiency of the parametrically excited magnons [26]. The drastic change at $\mu_0 H = 48$ mT in Fig. 4 supports that the primary mode switches between the exchange mode and dipole-exchange mode at this field. Figure 4 shows that the $\mu_0 H$ dependence of $\kappa(H)/\kappa_{max}$ is almost the same between the Pt/YIG bilayer and Pt/NiO/YIG trilayer when $H > H_{jump}$. In contrast, when $H < H_{jump}$, $\kappa(H)$ for the Pt/NiO/YIG trilayer is clearly larger than that for the Pt/YIG bilayer. This indicates that, in the Pt/NiO/YIG trilayer, the suppression of the spin-pumping efficiency due to the NiO insertion for the dipole-exchange magnons is more significant than that for the exchange magnons.

To further confirm the higher spin-pumping efficiency of the exchange magnons in the Pt/NiO/YIG trilayer, we plot κ as a function of $\mu_0 H$ and P_{in} in Fig. 5. In Fig. 5, the dashed curves in black represent $H_{jump}(P_{in})$, where the primary mode switches between exchange and dipole-exchange magnons. Figure 5 shows that κ of the dipole-exchange magnons, excited at $H > H_{jump}(P_{in})$, is almost identical between the Pt/YIG bilayer and Pt/NiO/YIG trilayer. In contrast, κ of the exchange magnons, excited at $H < H_{jump}(P_{in})$, is clearly different between the Pt/YIG bilayer and Pt/NiO/YIG trilayer for all P_{in}.

Our experimental finding is that the suppression of the spin-pumping efficiency due to the NiO insertion for the dipole-exchange magnons with the wave number of $k \sim 10^3 - 10^4$ cm^{-1} is more significant than that for the exchange magnons with $k \sim 10^5$ cm^{-1}, as shown in Figs. 4 and 5. In the YIG layer, the in-plane wavelength of the exchange magnons, excited by the parametric pumping, is several tens of nanometers and that of the dipole-exchange magnons is several tens of micrometers. Although an important role of the spin correlation length ξ in the spin transport through antiferromagnets has been suggested [4], $\xi = l[(T/T_N) - 1]^{-0.64} \sim 1$ nm at room temperature is orders of magnitude shorter than the wavelength of the parametrically excited magnons, where $l = 0.42$ nm and T_N is the Néel temperature [34], showing that the spin correlation is irrelevant to the observed difference between the spin pumping driven by the exchange and dipole-exchange magnons.

The difference in the spin-pumping efficiency between the exchange and dipole-exchange magnons in the Pt/NiO/YIG trilayer can be attributed to antiferromagnetic grain size effects. In a NiO film sputtered at room temperature, the

antiferromagnetic grain size is known to be below 20 nm [35–37]. In the Pt/NiO/YIG trilayer, the randomly oriented NiO grains induce spatially random exchange bias fields at the NiO/YIG interface, which act as a magnetic disorder in the YIG film. This disorder triggers two-magnon scattering and enhances the damping of magnons in the YIG layer [38]. The additional damping $\eta_{\rm tm}$ due to the two-magnon scattering is independent of the wavenumber of the magnons when the scatterer size is less than 20 nm [39]. Thus, the damping of the dipole-exchange magnons $\eta_{\rm de}$ and that of the exchange magnons $\eta_{\rm ex}$ can be approximated as $\eta_{\rm de}+\eta_{\rm tm}$ and $\eta_{\rm ex}+\eta_{\rm tm}$, respectively, in the presence of the two-magnon scattering due to the randomly oriented exchange bias. This indicates that the spin pumping driven by the parametric magnons is suppressed by the two-magnon scattering induced by inserting the NiO layer because the spin-pumping efficiency is inversely proportional to the damping η of magnons responsible for the spin pumping, $\kappa \propto 1/\eta$ [40]. Since $\eta_{\rm de}$ is clearly smaller than $\eta_{\rm ex}$ even when the frequency of the exchange and dipole-exchange magnons is the same [see Fig. 3(b)] [27], the change of the damping due to the two-magnon scattering of the dipole-exchange magnon, $(\eta_{\rm de}+\eta_{\rm tm})/\eta_{\rm de}$, is larger than that of the exchange magnon, $(\eta_{\rm ex}+\eta_{\rm tm})/\eta_{\rm ex}$. This shows that the suppression of the spin-pumping efficiency driven by the dipole-exchange magnons is more significant than that driven by the exchange magnons, consistent with the experimental result, shown in Fig. 4.

The spin pumping driven by parametric magnons is also expected to be affected by spin pinning. In a polycrystalline magnet, spins are pinned at the grain boundaries [41]. This effect pins the spins at the grain boundaries in the NiO layer. The spins in the YIG layer on top of the grain boundaries are also pinned due to the interface spin exchange coupling. Thus, under the microwave excitation, the precessional motion of the spins in both YIG and NiO layers is suppressed at the grain boundaries of the NiO layer. This pinning effect suppresses the spin pumping [42], especially driven by the dipole-exchange magnons, whose wavelength is three-orders of magnitude larger than the size of the antiferromagnetic grains.

IV. CONCLUSIONS

We studied the spin pumping in the Pt/NiO/YIG trilayer under the parametric excitation. The parametric excitation in the YIG layer creates magnons with nonzero wave numbers. The parametrically excited magnons emit a spin current into the antiferromagnetic NiO layer through the spin pumping, and the spin current is detected using the ISHE in the Pt layer. We found that the spin-pumping efficiency, defined as the ratio between the ISHE voltage to the microwave absorption intensity, of the Pt/NiO/YIG trilayer is about an order smaller than that of the Pt/YIG bilayer. The suppression of the spin-pumping efficiency due to the NiO insertion is consistent with the spin-current decay in the NiO layer. Furthermore, we found that the suppression of the spin-pumping efficiency depends on the wave number of the parametrically excited magnons. The wave-number dependence is attributed to the two-magnon scattering and spin pinning due to the antiferromagnetic grains in the NiO layer. These results provide insight into the understanding of the spin pumping into antiferromagnetic insulators.

ACKNOWLEDGMENTS

This work was supported by JSPS KAKENHI Grants No. 19K22131 and No. 19H00864, the Canon Foundation, the Asahi Glass Foundation, JGC-S Scholarship Foundation, and Spintronics Research Network of Japan (Spin-RNJ).

[1] I. Zutı, J. Fabian, and S. D. Sarma, Rev. Mod. Phys. **76**, 323 (2004).
[2] Y. Kajiwara, K. Harii, S. Takahashi, J.-I. Ohe, K. Uchida, M. Mizuguchi, H. Umezawa, H. Kawai, K. Ando, K. Takanashi *et al.*, Nature (London) **464**, 262 (2010).
[3] K. Uchida, J. Xiao, H. Adachi, J.-i. Ohe, S. Takahashi, J. Ieda, T. Ota, Y. Kajiwara, H. Umezawa, H. Kawai *et al.*, Nat. Mater. **9**, 894 (2010).
[4] W. Lin, K. Chen, S. Zhang, and C. L. Chien, Phys. Rev. Lett. **116**, 186601 (2016).
[5] H. Wang, C. Du, P. C. Hammel, and F. Yang, Phys. Rev. Lett. **113**, 097202 (2014).
[6] C. Hahn, G. De Loubens, V. V. Naletov, J. B. Youssef, O. Klein, and M. Viret, Europhys. Lett. **108**, 57005 (2014).
[7] H. Wang, C. Du, P. C. Hammel, and F. Yang, Phys. Rev. B **91**, 220410(R) (2015).
[8] Z. Qiu, J. Li, D. Hou, E. Arenholz, A. T. N'Diaye, A. Tan, K.-i. Uchida, K. Sato, S. Okamoto, Y. Tserkovnyak *et al.*, Nat. Commun. **7**, 12670 (2016).
[9] A. Prakash, J. Brangham, F. Yang, and J. P. Heremans, Phys. Rev. B **94**, 014427 (2016).
[10] W. Lin and C. L. Chien, Phys. Rev. Lett. **118**, 067202 (2017).
[11] D. Hou, Z. Qiu, J. Barker, K. Sato, K. Yamamoto, S. Vélez, J. M. Gomez-Perez, L. E. Hueso, F. Casanova, and E. Saitoh, Phys. Rev. Lett. **118**, 147202 (2017).
[12] Y.-M. Hung, C. Hahn, H. Chang, M. Wu, H. Ohldag, and A. D. Kent, AIP Adv. **7**, 055903 (2017).
[13] R. Khymyn, I. Lisenkov, V. S. Tiberkevich, A. N. Slavin, and B. A. Ivanov, Phys. Rev. B **93**, 224421 (2016).
[14] S. Takei, T. Moriyama, T. Ono, and Y. Tserkovnyak, Phys. Rev. B **92**, 020409(R) (2015).
[15] S. M. Rezende, R. L. Rodríguez-Suárez, and A. Azevedo, Phys. Rev. B **93**, 054412 (2016).
[16] T. Moriyama, M. Kamiya, K. Oda, K. Tanaka, K.-J. Kim, and T. Ono, Phys. Rev. Lett. **119**, 267204 (2017).
[17] R. Lebrun, A. Ross, S. Bender, A. Qaiumzadeh, L. Baldrati, J. Cramer, A. Brataas, R. Duine, and M. Kläui, Nature (London) **561**, 222 (2018).
[18] R. Iguchi, K. Ando, R. Takahashi, T. An, E. Saitoh, and T. Sato, Jpn. J. Appl. Phys. **51**, 103004 (2012).
[19] E. Saitoh, M. Ueda, H. Miyajima, and G. Tatara, Appl. Phys. Lett. **88**, 182509 (2006).

[20] T. Kimura, Y. Otani, T. Sato, S. Takahashi, and S. Maekawa, Phys. Rev. Lett. **98**, 156601 (2007).
[21] S. O. Valenzuela and M. Tinkham, Nature (London) **442**, 176 (2006).
[22] K. Uchida, S. Takahashi, K. Harii, J. Ieda, W. Koshibae, K. Ando, S. Maekawa, and E. Saitoh, Nature **455**, 778 (2008).
[23] Y. Tserkovnyak, A. Brataas, and G. E. W. Bauer, Phys. Rev. Lett. **88**, 117601 (2002).
[24] K. Ando, Semicond. Sci. Technol. **29**, 043002 (2014).
[25] C. Sandweg, Y. Kajiwara, K. Ando, E. Saitoh, and B. Hillebrands, Appl. Phys. Lett. **97**, 252504 (2010).
[26] M. Fukami, Y. Tateno, K. Sekiguchi, and K. Ando, Phys. Rev. B **93**, 184429 (2016).
[27] G. Wiese, P. Kabos, and C. E. Patton, Phys. Rev. B **51**, 15085 (1995).
[28] H. Hayashi and K. Ando, Phys. Rev. Lett. **121**, 237202 (2018).
[29] C. W. Sandweg, Y. Kajiwara, A. V. Chumak, A. A. Serga, V. I. Vasyuchka, M. B. Jungfleisch, E. Saitoh, and B. Hillebrands, Phys. Rev. Lett. **106**, 216601 (2011).
[30] H. Kurebayashi, O. Dzyapko, V. Demidov, D. Fang, A. Ferguson, and S. Demokritov, Appl. Phys. Lett. **99**, 162502 (2011).
[31] M. Sparks, *Ferromagnetic-Relaxation Theory* (McGraw-Hill, New York, 1964).
[32] X. Lang, W. Zheng, and Q. Jiang, Nanotechnology **18**, 155701 (2007).
[33] T. Neumann, A. A. Serga, V. I. Vasyuchka, and B. Hillebrands, Appl. Phys. Lett. **94**, 192502 (2009).
[34] T. Chatterji, G. J. McIntyre, and P.-A. Lindgard, Phys. Rev. B **79**, 172403 (2009).
[35] H.-L. Chen, Y.-M. Lu, and W.-S. Hwang, Thin Solid Films **498**, 266 (2006).
[36] G. Vallejo-Fernandez, L. Fernandez-Outon, and K. O'Grady, J. Phys. D : Appl. Phys. **41**, 112001 (2008).
[37] A. C. Gandhi, J. Pant, S. D. Pandit, S. K. Dalimbkar, T.-S. Chan, C.-L. Cheng, Y.-R. Ma, and S. Y. Wu, J. Phys. Chem. C **117**, 18666 (2013).
[38] H. Sakimura, A. Asami, T. Harumoto, Y. Nakamura, J. Shi, and K. Ando, Phys. Rev. B **98**, 144406 (2018).
[39] U. Hoeppe and H. Benner, Phys. Rev. B **71**, 144403 (2005).
[40] H. Sakimura, T. Tashiro, and K. Ando, Nat. Commun. **5**, 5730 (2014).
[41] J. Pankert, J Magn. Magn. Mater. **138**, 45 (1994).
[42] R. Takemasa, Y. Tateno, and K. Ando, Appl. Phys. Lett. **110**, 042404 (2017).